Role of CD40 and ADAMTS13 in von Willebrand factor-mediated endothelial cell–platelet–monocyte interaction

Miruna Popa[a], Sibgha Tahir[a], Julia Elrod[a], Su Hwan Kim[a], Florian Leuschner[b,c], Thorsten Kessler[d], Peter Bugert[e], Ulrich Pohl[f,g], Andreas H. Wagner[a,1,2], and Markus Hecker[a,c,1]

[a]Department of Cardiovascular Physiology, Heidelberg University, 69120 Heidelberg, Germany; [b]Internal Medicine III, University Clinics Heidelberg, 69120 Heidelberg, Germany; [c]DZHK (German Centre for Cardiovascular Research), Partnersite Heidelberg/Mannheim, 69120 Heidelberg, Germany; [d]Department of Cardiovascular Diseases, German Heart Centre Munich, Technical University Munich, 80636 Munich, Germany; [e]German Red Cross Blood Service Baden-Württemberg-Hessen, Institute of Transfusion Medicine and Immunology, 68167 Mannheim, Germany; [f]Walter Brendel Centre of Experimental Medicine, Biomedical Center of Ludwig Maximilian University of Munich (LMU), Ludwig Maximilian University of Munich, 82152 Munich Germany; and [g]DZHK (German Centre for Cardiovascular Research), Partnersite Munich, 80636 Munich, Germany

Edited by Jason G. Cyster, University of California, San Francisco, CA, and approved May 4, 2018 (received for review January 24, 2018)

Monocyte extravasation into the vessel wall is a key step in atherogenesis. It is still elusive how monocytes transmigrate through the endothelial cell (EC) monolayer at atherosclerosis predilection sites. Platelets tethered to ultra-large von Willebrand factor (ULVWF) multimers deposited on the luminal EC surface following CD40 ligand (CD154) stimulation may facilitate monocyte diapedesis. Human ECs grown in a parallel plate flow chamber for live-cell imaging or Transwell permeable supports for transmigration assay were exposed to fluid or orbital shear stress and CD154. Human isolated platelets and/or monocytes were superfused over or added on top of the EC monolayer. Plasma levels and activity of the ULVWF multimer-cleaving protease ADAMTS13 were compared between coronary artery disease (CAD) patients and controls and were verified by the bioassay. Two-photon intravital microscopy was performed to monitor CD154-dependent leukocyte recruitment in the cremaster microcirculation of ADAMTS13-deficient versus wild-type mice. CD154-induced ULVWF multimer–platelet string formation on the EC surface trapped monocytes and facilitated transmigration through the EC monolayer despite high shear stress. Two-photon intravital microscopy revealed CD154-induced ULVWF multimer–platelet string formation preferentially in venules, due to strong EC expression of CD40, causing prominent downstream leukocyte extravasation. Plasma ADAMTS13 abundance and activity were significantly reduced in CAD patients and strongly facilitated both ULVWF multimer–platelet string formation and monocyte trapping in vitro. Moderate ADAMTS13 deficiency in CAD patients augments CD154-mediated deposition of platelet-decorated ULVWF multimers on the luminal EC surface, reinforcing the trapping of circulating monocytes at atherosclerosis predilection sites and promoting their diapedesis.

endothelial cells | coronary artery disease | ADAMTS13 | von Willebrand factor | CD40

Atherosclerosis is a chronic inflammatory disease of middle-sized and large conduit arteries. Formation of atherosclerotic lesions starts in early life and progresses with advancing age, gradually leading to arterial stenosis and occlusion. Typical predilection sites for atherosclerotic plaques are bifurcations and curvatures of conduit arteries where disturbed blood flow facilitates endothelial cell (EC) dysfunction, which in turn enables the recruitment and diapedesis of circulating immune cells, predominantly monocytes and T lymphocytes (1). Although atherogenesis is a complex process comprising ECs, vascular smooth muscle cells (SMCs), and a large variety of leukocytes, the critical determinants of atherosclerotic lesion formation are considered to be monocyte-derived macrophages (2). However, the process by which monocytes enter the arterial vessel wall under arterial flow conditions remains elusive. In particular, it is not known how these leukocytes manage to adhere to the surface of the arterial EC monolayer and transmigrate through it.

This process may be strongly facilitated by a CD40-dependent mechanism. It is well known that the CD40–CD40 ligand (CD154) interaction (3) is one of the major proinflammatory pathways involved in atherogenesis. The CD40–CD154 receptor–ligand dyad is known to be involved in all stages of atherosclerosis, as CD40 and CD154 are coexpressed by ECs, vascular SMCs, and macrophages in atherosclerotic plaques, most prominently in the shoulder region (4). CD154-expressing activated platelets may orchestrate the inflammatory CD40–CD154–dependent process in atherosclerotic lesions, as platelets account for >95% of soluble CD154 (sCD154) in the circulation (5).

von Willebrand factor (vWF) is a multimeric plasma glycoprotein produced by ECs and megakaryocytes that is involved in both primary and secondary hemostasis. Normally, EC activation or injury results in the release of these ultra-large vWF (ULVWF) multimers, which have a much higher thrombogenic potential than vWF monomers (6). CD154 binding to endothelial cell CD40 induces the release of ULVWF multimers from

Significance

In this study we have identified a mechanism that links pathophysiological ADAMTS13 deficiency to innate immunity and hemostasis by facilitating monocyte extravasation as a prerequisite for their subsequent on-site differentiation into proinflammatory macrophages under conditions of both physiological laminar flow and disturbed reduced flow, e.g., as occurs at atherosclerosis predilection sites. Our bioassay approach using patients' plasma may become a useful diagnostic tool to assess ADAMTS13 activity ex vivo under conditions of near-physiological to atherosclerosis-prone arterial blood flow, which seems to be more relevant than the conventional static FRET-based assay method.

Author contributions: M.P., U.P., A.H.W., and M.H. designed research; M.P., S.T., J.E., and S.H.K. performed research; F.L., T.K., and P.B. collected blood samples; M.P., F.L., T.K., P.B., U.P., A.H.W., and M.H. analyzed data; and M.P., A.H.W., and M.H. wrote the paper.

The authors declare no conflict of interest.

This article is a PNAS Direct Submission.

[1]A.H.W. and M.H. contributed equally to this work.

[2]To whom correspondence should be addressed. Email: a.wagner@physiologie.uni-heidelberg.de.

This article contains supporting information online at www.pnas.org/lookup/suppl/doi:10.1073/pnas.1801366115/-/DCSupplemental.

Published online May 23, 2018.

Weibel–Palade bodies (WPBs) and their deposition on the EC surface. This release from the WPBs is calcium mediated through consecutive TRAF6, Src kinase, and PLCγ1 activation both under static conditions and in response to arterial shear stress (7).

Under physiological conditions, deposition of ULVWF multimers on the EC surface is efficiently impaired by plasma ADAMTS13, a protease that controls the length of ULVWF multimers by cleaving them into smaller, less active fragments 3 to 15 μm in length that are released into the circulation (8). However, under conditions of low plasma ADAMTS13 activity ULVWF multimers may persist under flow and constitute a thrombogenic EC surface (9). ADAMTS13 shows the highest expression in ECs and hepatic stellate cells (10). Severe deficiency in ADAMTS13 plasma activity results in thrombotic thrombocytopenic purpura (TTP). During acute episodes of TTP, both congenital and acquired ADAMTS13 deficiency lead to a severe loss of ADAMTS13 protein or activity to <5% of normal plasma values, hence causing disseminated microvascular thrombosis followed by acute organ failure (6, 11).

Interestingly, deficiency in ADAMTS13 is not restricted to TTP. Several lines of evidence indicate that moderate ADAMTS13 deficiency is associated with cardiovascular disease, but direct proof that ADAMTS13 deficiency causes prolonged deposition of ULVWF multimers on the luminal EC surface at atherosclerosis predilection sites, and thus increased recruitment and transmigration of monocytes, is lacking. Therefore, we analyzed whether CD154-induced EC release of ULVWF multimers facilitates platelet–monocyte interaction under flow conditions resembling those occurring at atherosclerosis predilection sites in vitro and the role that ADAMTS13 deficiency plays therein. Moreover, we determined ADAMTS13 levels in the plasma of patients with coronary artery disease (CAD) and related this to its ULVWF multimer-resolving effect in the aforementioned bioassay system. Finally, we studied ULVWF multimer–platelet string formation in ADAMTS13-deficient mice by two-photon intravital microscopy.

Results

ULVWF Multimer Formation: Effects of Shear Stress. CD154-induced ULVWF multimer formation and deposition on human ECs was studied under low unidirectional shear stress (2.5–10 dyn/cm^2), as found in conduit arteries at atherosclerosis predilection sites. ULVWF multimers were observed on the EC surface within 2 min of applying histamine (1 μmol/L) or bradykinin (0.1 μmol/L) and became further elongated. They were oriented parallel to the flow direction and reached a mean length of 190 μm. Platelets specifically adhered only to ULVWF multimers but not to ECs, forming beads-on-a-string structures. These were quite stable due to the constant formation of new strings and elongation processes, which attracted more circulating platelets to the ULVWF multimers. On average, ULVWF multimer–platelet strings had a half-life clearly exceeding 10 min (*SI Appendix*, Fig. S1).

Upon stimulation of human umbilical vein endothelial cells (HUVECs) with 200 ng/mL soluble trimeric recombinant CD154 (sCD154) at 10 dyn/cm^2, a prominent deposition of platelet-decorated ULVWF multimers on the EC surface was observed within 2 min, as shown in Fig. 1 *A* and *B*, which matched the effects of bradykinin in both stability and length (183.4 ± 28.6 μm, mean ± SEM, $n = 7$). In some experiments, the length of CD154-induced ULVWF multimer–platelet strings exceeded 700 μm. Immunofluorescence analyses further revealed a sCD154-mediated intracellular clustering of WPBs similar to those induced by bradykinin. This fusion of individual WPBs was not observed in nonstimulated ECs exposed to unidirectional shear stress (*SI Appendix*, Fig. S2*A*).

As activated platelets are known to present CD154 on their surface immediately upon thrombin stimulation (12), they were used as a source of membrane-bound CD154. Superfusion of HUVECs with thrombin-activated platelets elicited a significant threefold increase in ULVWF multimer release and deposition on their surface similar in extent to that seen with sCD154 or bradykinin stimulation. Again, the stability of these strings was comparable, while the length and especially density of the tethered platelets appeared to be more pronounced (*SI Appendix*, Fig. S2 *B* and *C*). To demonstrate the specificity of platelet-bound CD154 in string formation, a neutralizing anti-CD154 antibody (TRAP1) was employed, which essentially reduced string formation to the level of the nonstimulated control (Fig. 1 *A* and *B*).

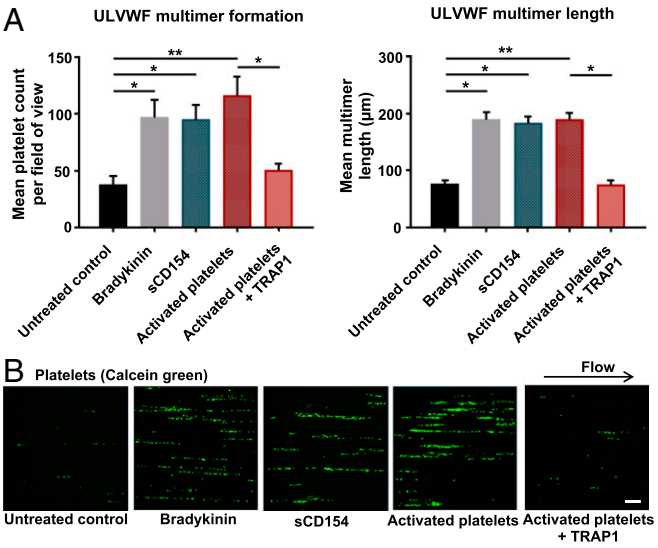

Fig. 1. CD154-induced ULVWF multimer formation. HUVECs exposed to 10 dyn/cm^2 were treated with 200 ng/mL trimeric recombinant sCD154, thrombin-activated platelets (2 × 10^6 cells/mL), thrombin-activated platelets treated with TRAP1 antibody, or 100 nmol/L bradykinin as a positive control. For activation, platelets were treated with 0.25 U/mL thrombin for 10 min and subsequently were incubated with 1 μmol/L hirudin for 10 min at room temperature to inactivate thrombin present in the cell suspension. For neutralization of membrane-bound CD154, activated platelets were incubated with 40 μg/mL TRAP1 antibody for 90 min at room temperature. (*A*) Quantification of ULVWF multimer formation and length. $n = 4$–9, $*P < 0.05$, $**P < 0.01$. (*B*) Representative snapshots from live-cell imaging. Platelets are seen as green dots aligned into string-like structures on the EC surface. (Scale bars: 50 μm.)

Effect of the CD40/CD154 Interaction on Monocyte Recruitment to ECs and Extravasation in the Presence of Shear Stress. The addition of human isolated and fluorescence dye-labeled monocytes to the perfusion system resulted in their rapid arrest by ULVWF multimer-bound platelets (*SI Appendix*, Fig. S3 *A*–*G*) and firm tethering to the EC surface within the first 5–10 min post stimulation with bradykinin (0.1 μmol/L). Occasionally, monocyte rolling from one platelet to the next was observed. Monocytes initially recruited to the platelet-decorated ULVWF multimers started to firmly tether directly to the ECs. Even if the multimer eventually detached from the EC surface, monocytes maintained their relative position in the field of view (an example is shown in *SI Appendix*, Fig. S3 *G* and *H*). Next HUVECs were stimulated with 200 ng/mL sCD154 or thrombin-activated platelets (2 × 10^6/mL), and monocyte recruitment was monitored for 1 h. Both stimuli led to prominent ULVWF multimer deposition on the EC surface which persisted for the entire observation period. Moreover, monocytes tethered rapidly to CD154-induced ULVWF multimers (Fig. 2 *A* and *B*) by preferentially interacting directly with the ULVWF multimer-bound platelets (*SI Appendix*, Fig. S4 *A* and *B*).

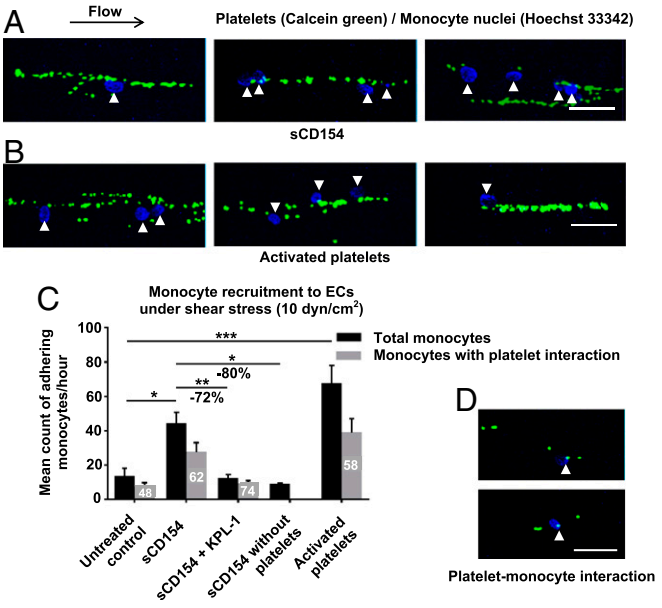

Fig. 2. CD154-induced monocyte recruitment to ULVWF multimers. HUVECs were exposed to laminar shear stress and were treated with either sCD154 or thrombin-activated platelets (green). Monocytes (blue) were added to the superfusate. (*A* and *B*) Fluorescently labeled monocytes adhered to platelet-decorated ULVWF multimers within the first 5–10 min of perfusion with preferential binding of monocytes to ULVWF multimers. Shown are representative images of sCD154 (*A*; $n = 8$) and activated platelets (*B*; $n = 6$) experiments using blood cells from different donors. (Magnification: 20×.) (Scale bars: 50 μm.) White arrowheads mark adhered monocytes. (*C*) Quantification of monocyte recruitment to untreated HUVECs and to HUVECs stimulated with sCD154 and activated platelets at 10 dyn/cm^2. As control, monocytes were incubated with PSGL-1 neutralizing KPL-1 antibody and were perfused over sCD154-activated HUVECs. Black bars represent the total number of recruited monocytes recorded in the defined time frame. Gray bars represent the fraction of those monocytes showing direct platelet interaction. White numbers on the gray bars represent the percentage of monocytes with platelet interaction relative to the total number of monocytes for each condition. $n = 3$–6, $^*P < 0.05$, $^{**}P < 0.01$, $^{***}P < 0.001$. Monocyte–platelet interaction was defined as monocytes attached to at least one platelet, as shown by arrowheads in *D*. (Magnification: 20×.) (Scale bar: 50 μm.)

SI Appendix, Fig. S4*C* shows a ULVWF multimer densely packed with green fluorescent platelets on which several blue fluorescent monocytes are trapped. Quantification of the monocyte–platelet interaction revealed a marked (3.3-fold) increase following exposure of the HUVECs to sCD154 and in particular to activated platelets (Fig. 2 *C* and *D*). Pretreatment of the monocytes with a neutralizing anti–PSGL-1 antibody (KPL-1) significantly reduced monocyte recruitment by 72% (Fig. 2*C*), corresponding to the level of the unstimulated control and indicating that PSGL-1 plays a pivotal role in monocyte trafficking to the EC surface in this model (13, 14).

Ranging from the untreated (48%) to the stimulated control (74%), on average 60% of monocytes recruited to the ECs showed direct interaction with ULVWF multimer-bound platelets (Fig. 2*C* and *SI Appendix*, Fig. S3), while superfusion of stimulated HUVECs in the absence of platelets strongly reduced monocyte trafficking by 80%, indicating that platelets are directly involved in monocyte recruitment under arterial shear stress conditions (10 dyn/cm^2). Next, platelet–monocyte interactions were visualized by reflection interference contrast microscopy (RICM). *SI Appendix*, Fig. S5 shows several adhesion patterns of monocytes interacting directly with platelets aligned onto ULVWF multimers. Monocytes interacted either with single platelets (*SI Appendix*, Fig. S5*C*) or with densely decorated ULVWF multimers, where they were situated either at the upstream end (*SI Appendix*, Fig. S5*D*) or in the middle portion of the ULVWF multimer–platelet string (*SI Appendix*, Fig. S5*E*). Others were trapped in densely decorated ULVWF multimers, being flanked by platelets in all directions (*SI Appendix*, Fig. S5*F*). RICM images thus clearly demonstrate direct platelet–monocyte interactions at the level of the ULVWF multimers. RICM also allowed visualization of the EC monolayer at different levels and thus monocyte–EC interactions at different stages of diapedesis (*SI Appendix*, Fig. S6), suggesting that monocytes interacting with platelets were not solely bound to ULVWF multimers but actively approached EC adherens junctions and started to transmigrate.

Next, monocyte transmigration was evaluated and quantified using a modified Boyden chamber. By imposing chronic multidirectional orbital shear stress (3–4 dyn/cm^2) (7, 15) on cultured HUVECs, a marked release from and net-like formation of ULVWF multimers on the EC surface was documented after sCD154 stimulation; histamine served as a positive control (Fig. 3*A*). Confocal microscopy visualized platelets and monocytes tethered to the ULVWF multimers released by the HUVECs upon sCD154 stimulation (Fig. 3*B*). Moreover, stimulation with sCD154 or histamine led to a significant three- to fourfold increase in monocyte transmigration after 24 h (Fig. 3*C*).

As a proof of concept, ULVWF multimer–platelet string formation through stimulation of CD40 on ECs and the subsequent attraction of leukocytes was studied in vivo in cremaster venules of wild-type and ADAMTS13-knockout mice ($n = 6$). Following injection of fluorescent dye-labeled platelets in ADAMTS13-knockout mice, the formation of ULVWF multimer–platelet strings with an average length of 20.1 ± 9.7 μm ($n = 3$) could be identified at a ratio of 0.9 ± 0.2 strings per venule (visualized in 5–10 venules per experiment). Topical application of recombinant sCD154 significantly increased the number of strings to 2.2 ± 0.7 per venule ($P < 0.01$; $n = 3$) but did not significantly alter their apparent length. During string formation leukocytes started to attach to the platelets located on the strings, often extending to adjacent sites without any labeled platelets. Leukocyte attachment was followed by their extravasation, which started in the vascular wall region where the ULVWF multimer–platelet string had originally formed. Fig. 4 *D* and *F* show such a string with the attachment of leukocytes and extravasation of two leukocytes. In contrast, some (but significantly fewer) ULVWF multimer–platelet strings were observed in wild-type control vessels (Fig. 4 *C* and *D*) because of the presence of enzymatically active ADAMTS13 in the blood.

ADAMTS13 Plasma Activity and Concentration in CAD. Finally, we investigated whether there are differences in ADAMTS13 plasma levels between patients with CAD and healthy individuals. To address this question, three groups of interest were defined: a young control population ($n = 41$), a CAD patient cohort ($n = 70$; the inclusion criterion was angiographic evidence of ≥25% stenosis in a relevant coronary artery), and an age-matched control group ($n = 50$). Table 1 shows the mean age and gender distributions of the analyzed groups. Perfect age matching of the CAD group and the aged control group with documented absence of cardiovascular diseases proved to be complicated because CAD prevalence in humans increases with age (16). Thus, it was difficult to find a sufficient number of individuals without evidence of CAD in daily clinical practice. Patient baseline characteristics are summarized in Table 2. Control individuals had no documented history of any cardiovascular disease, were nonsmokers, and did not take any medication.

Plasma ADAMTS13 was quantified by measuring both ADAMTS13 activity and protein using commercially available kits with high interassay precision (*SI Appendix*, Table S1). According to these analyses, patients with CAD had significantly

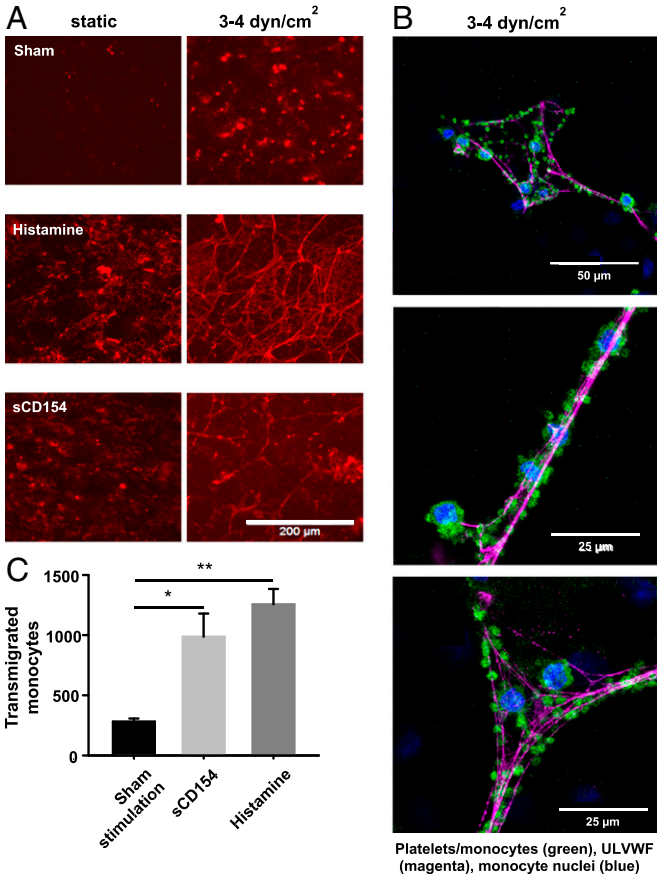

Fig. 3. Transmigration of monocytes under orbital shear stress conditions upon sCD154 stimulation. (*A*) HUVECs were stimulated with sCD154 (200 ng/mL) or histamine (5 μmol/L) or were sham-stimulated for 20 min under static conditions or upon application of orbital shear stress (3–4 dyn/cm^2), leading to the formation of ULVWF multimers stained in red. (*B*) Confocal fluorescence microscopy images of platelets (CD42b) and monocytes (CD14) adhering to ULVWF multimers. Shown are maximum projections of several focal planes above the HUVEC layer (green = CD14, CD42b; magenta = vWF; blue = DAPI). HUVECs were cultured on glass-bottomed dishes and were stimulated with 200 ng/mL sCD154 combined with orbital shear stress application. Note that some DAPI-positive nuclei, not associated with ULVWF multimers, belong to the HUVECs. (*C*) Quantification of transmigrated monocytes upon sCD154 (200 ng/mL), histamine (5 μmol/L), and sham (PBS) stimulation. Stimuli and platelets (3×10^5) were removed after 10 min; then fresh medium containing monocytes (1×10^6) was added, and orbital shear stress (3–4 dyn/cm^2) was applied. Transmigrated monocytes were quantified using a Neubauer improved cell counting chamber after 24 h. $n = 6$, $^*P < 0.05$, $^{**}P < 0.01$.

reduced plasma ADAMTS13 activity and antigen levels compared with both control groups (Fig. 5). A statistical data summary of all analyzed groups is presented in Table 3. Overall ADAMTS13 activity in CAD patients was significantly reduced, by 23% and 10% compared with the young and aged controls, respectively. Activity levels in all three groups correlated almost perfectly with ADAMTS13 antigen levels (*SI Appendix*, Fig. S6). Since CAD severity and coronary artery stenosis increase with the progression of atherosclerosis, we investigated whether ADAMTS13 levels depend on the stage of the disease, acute myocardial infarction (AMI), or the T-786C SNP of the *NOS-3* gene which increases the relative risk of contracting CAD (17) by causing endothelial dysfunction. However, there was no statistically significant correlation of either ADAMTS13 plasma activity or concentration with the severity of CAD, acute coronary syndrome, or the T-786C SNP of the *NOS-3* gene (*SI Appendix*, Fig. S8 *A–D*).

What are the consequences of the moderately reduced plasma levels of ADAMTS13 in the patients with CAD, i.e., are they still sufficient to prevent the deposition and accumulation of adhesive ULVWF multimers on the luminal surface of the ECs? To answer this question, the established in vitro superfusion of cultured HUVECs was employed as a bioassay system under standardized conditions (10 dyn/cm^2 unidirectional shear stress, 0.1 μmol/L bradykinin). First, titration experiments using serial dilutions of selected platelet-poor plasma stocks were performed to determine a cutoff value below which the ULVWF multimers are no longer effectively cleaved. These stocks were prepared to obtain defined ADAMTS13 concentrations (1,000, 750, 500, and 350 ng/mL) in the reconstituted blood solution that corresponded to the range found in the patients and controls (350–1,000 ng/mL). This was necessary because the activity of human recombinant ADAMTS13 turned out to be too low.

As shown in Fig. 6, superfusing activated ECs with ADAMTS13 in decreasing concentrations enabled an exponential increase in ULVWF multimer–platelet string formation on the surface of the ECs due to reduced cleavage (cutoff value <600 ng/mL) that was significantly more pronounced at ADAMTS13 concentrations found in the plasma of patients with CAD than at the concentrations found in the two control groups. ULVWF multimer lengths gradually increased from 14.9 ± 1.9 μm (1,000 ng/mL) to 81.3 ± 8.1 μm (350 ng/mL). Consistent with this, platelet adherence was 10.2-fold higher at 350 ng/mL than at 1,000 ng/mL. The arrows in Fig. 6 *D* and *E* indicate the measured mean ADAMTS13 concentrations in young controls (823.7 ng/mL) and in CAD patients (636.3 ng/mL) using the FRET assay, suggesting that plasma obtained from patients with CAD will lead to an increased deposition of ULVWF multimer–platelet strings on the surface of the HUVECs under our assay conditions.

Therefore, pooled native plasma from patients with CAD ($n = 24$) and from young healthy donors ($n = 20$) was tested in the bioassay. As shown in Fig. 7, there was a marked (fourfold) and significant increase in platelet tethering to the ULVWF multimers as well as in ULVWF multimer length when the plasma of the patients with CAD was employed. When these values are interpolated into the titration curves shown in Fig. 6 *D* and *E*, an ADAMTS13 concentration resulted which was similar to the average plasma activity and concentration previously measured in patients with CAD and in healthy donors.

Finally, HUVECs were treated either with 200 ng/mL sCD154 or with thrombin-activated platelets and were superfused with a reconstituted blood solution containing 350 ng/mL ADAMTS13. As shown in *SI Appendix*, Fig. S9, there was prominent formation of stable ULVWF multimer–platelet strings of intermediate length (up to 40 μm) under these conditions, and monocytes firmly adhered to the platelet-decorated ULVWF multimers, as described above. This suggests that ULVWF multimer–platelet strings formed in the presence of the pooled plasma from patients with CAD are stable enough to facilitate monocyte recruitment.

Discussion

The current study investigated the atherogenic potential of CD40/CD154 interaction by assessing the functional impact of CD154-induced ULVWF multimer formation on platelet-dependent monocyte recruitment. Our findings suggest that platelets attached to ULVWF multimers facilitate the trapping of circulating monocytes at sites of EC activation and promote their infiltration into the vessel wall. Furthermore, the current study provides an answer to the thus far unsolved question whether the moderate ADAMTS13 deficiency frequently reported in CAD patients is clinically relevant by promoting ULVWF multimer formation and monocyte recruitment.

Previous in vivo studies revealed that blocking CD40–CD154 signaling reduces atherosclerotic lesion size and the presence of

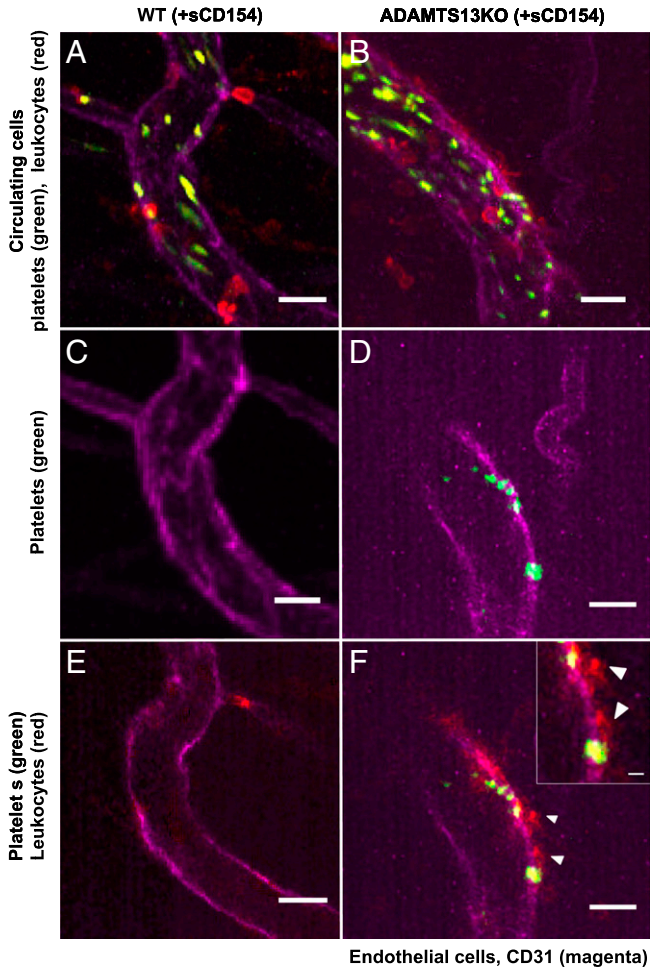

Fig. 4. Two-photon intravital microscopy in wild-type and ADAMTS13-knockout mice. Shown are representative images of a venule observed in a wild-type control mouse (*A*, *C*, and *E*) and in a ADAMTS13-knockout (ADAMTS13KO) mouse (*B*, *D*, and *F*) after 20 min of sCD154 stimulation followed by platelet and leukocyte labeling. Platelets are depicted in green (CFDA), leukocytes in red (CD45), and endothelium in magenta (CD31). *A* and *B* are z-stacks of several optic sections taken over a total period of 30 s showing comparable amounts of circulating/adhering platelets and leukocytes during that period of time in both vessels. *C* and *D* show the presence or absence of a permanent ULVWF multimer–platelet string in one focal plane only (notice the formation of the ULVWF multimer-associated platelet string in the ADAMTS13-deficient mouse in this particular vessel). *E* and *F* present a merged image of all channels taken simultaneously in one focal plane. In the ADAMTS13-deficient venule (*F*), the first signs of leukocyte transmigration can be observed in the string area. The *Inset* shows extravasation of leukocytes (white arrowheads). (Scale bars: 20 μm; 5 μm in *Inset*.) Note that the leukocyte outside the large control vessel in *A* has not transmigrated but is located in a side branch (compare *A* with *C* and *E*).

macrophages and T lymphocytes in the plaque (4, 18). This effect has been attributed thus far to an increased expression of adhesion molecules, cytokines, and chemokines by ECs. The present study proposes a mechanism by which CD154 contributes to monocyte recruitment under arterial shear stress conditions by showing that CD154-induced ULVWF multimer–platelet strings reveal high adhesive potential toward circulating monocytes even at a shear stress of 10 dyn/cm^2.

Strong vWF secretagogues induced the formation of ULVWF multimers, which remained anchored to the activated endothelium particularly under conditions of ADAMTS13 deficiency. Under flow conditions platelets attached firmly to these ULVWF multimers by an instant trapping mechanism without any rolling movement, forming characteristic beads-on-a-string–like structures on the EC surface. These observations are consistent with previous reports (19) and are known to be based on the high-strength bonds between platelet GpIbα and the vWF A1 domain (20). When ADAMTS13 is absent, ULVWF multimer–platelet strings are remarkably stable despite arterial flow conditions and even upon flow reversal remained anchored to the EC surface, just reversing their orientation. This high stability toward shear forces, which presumably is due to self-assembly of the ULVWF multimers into net-like structures on the EC surface (21), may allow such long (herein up to 1,800 μm) ULVWF multimer–platelet strings to persist at atherosclerosis predilection sites as well as in stenotic arterial segments (20). This conclusion is also supported by our intravital microscopy observations on a high number of strings in the ADAMTS13-deficient mice.

Our finding that platelet adherence to ULVWF multimers is greater at arterial (10 dyn/cm^2) than at venous (2.5 dyn/cm^2) shear stress is not unprecedented but reinforces the notion that shear stress is a pivotal force triggering the transformation of inactive globular vWF into hyperactive ULVWF multimers (*SI Appendix*, Fig. S10) (22). However, the average length of the ULVWF multimers remained the same. This shear stress-dependent conformational transition of the ULVWF multimers would counteract high hydrodynamic forces at sites of vascular injury by causing increased exposure of platelet-binding sites on the multimers, enabling platelet tethering even at high shear rates (23).

Platelets account for 95% of circulating CD154, which they immediately translocate to their surface upon activation and release into the circulation as sCD154 (12). Thrombin-activated platelets were therefore used as a physiological source of membrane-bound CD154 in the present study. Elevated levels of sCD154 are found in patients with coronary heart disease (24), unstable angina (25), and AMI (26) and are believed to be a marker of platelet activation and a possible predictor of adverse cardiovascular events (27). Activated platelets are a common phenomenon in patients with atherosclerosis (13). They are thought to become activated by disturbed blood flow, by interacting with activated endothelium, or by cytokines released during thromboembolic events and from inflamed tissues in systemic inflammation (28). These conditions commonly found in cardiovascular disease may thus explain why platelets in atherosclerosis express elevated levels of P-selectin and CD154.

Treatment of ECs with both recombinant sCD134 and platelet-derived CD154 induced a prominent release and deposition of ULVWF multimers to which circulating platelets immediately tethered. sCD154 had an effect similar to that of bradykinin, confirming it to be a potent vWF secretagogue (7), and this effect was specific, as demonstrated by incubating thrombin-activated platelets with TRAP-1, a commonly employed neutralizing antibody (12). Monocytes firmly adhered to these ULVWF multimers almost exclusively through interacting with platelets rather than with vWF (29) or the cultured ECs. Platelets thus seem to facilitate monocyte recruitment by forming a "sticky" platform, which helps monocytes come to a complete arrest despite the high shear rate. These findings are consistent with previous reports about circulating leukocytes interacting with platelet-decorated ULVWF multimers both in vitro (30) and in vivo (31). Since neutrophils are also known to interact with platelets (32–34), it was crucial to confirm that the visualized cells were monocytes. FACS analysis constantly revealed a monocyte purity of 94%, and during live-cell imaging the fluorescent dye-labeled cells revealed an ellipsoidal nuclear morphology or kidney-shaped nuclei, which are characteristic of monocytes. Furthermore, an artificial shift toward a certain monocyte subtype induced by magnetic bead isolation could be excluded, since isolated monocytes showed a normal subset distribution (35).

Table 1. Age and gender distribution of CAD patients and control groups

	n	Mean age, y ± SD	Minimum age, y	Maximum age, y	No. male (%)	No. female (%)
Young controls	41	27.2 ± 9.9	20	48	23 (56.1)	18 (43.9)
Aged controls	50	63.1 ± 3.3*	58	71	34 (68.0)	16 (32.0)
CAD patients	70	70.3 ± 11.7**	36	90	45 (64.3)	25 (35.7)

Differences in gender distribution among groups were not statistically significant ($P = 0.4914$, χ^2 test).
*$P < 0.001$ vs. young controls.
**$P < 0.001$ vs. aged controls.

The trapping mechanism, in which monocytes rolling over the platelet-decorated ULVWF multimers were observed only infrequently, deviates from the widely accepted multistep paradigm for leukocyte recruitment to ECs observed in postcapillary venules (14, 36). In contrast to other leukocytes, monocytes seem to have a strong binding affinity to ULVWF multimer-bound platelets, which results in their immediate arrest and not in a rolling mechanism. It is conceivable that the rolling paradigm does not apply to EC–monocyte interactions at sites of inflammation in conduit arteries, as here the shear rates are far higher than in postcapillary venules, making the initial rolling step barely possible. Another reason why monocyte binding to platelets is so strong may be that this P-selectin–PSGL-1 interaction (30) depends on the density of P-selectin on the platelet surface, which is much higher than on ECs (37). In fact, Kuligowski et al. (38) found that neutrophils come to an immediate arrest on glomerular ECs in a P-selectin–PSGL-1–dependent manner without showing any rolling motions.

Moreover, RICM and transmigration experiments allowed detailed analysis of platelet–monocyte–EC interactions and transmigration under flow. Within minutes after firm adhesion to the platelets, monocytes changed their shape by building pseudopodia, which might represent a first step toward transmigrating through the EC monolayer. In fact, P-selectin–dependent platelet–monocyte interactions are known to induce monocyte activation by increasing the affinity of monocytic β1- and β2-integrins toward VCAM-1 and ICAM-1 on the luminal EC surface (39). Furthermore, platelets deposit chemokines such as RANTES, CXCL5, and platelet factor-4 on the endothelium, which promote leukocyte arrest and transmigration (40). Like van Gils et al. (41), we observed that platelets dissociate from the monocytes once they start to transmigrate through the EC monolayer, presumably due to PSGL-1 redistribution and mechanical stress.

Using two-photon intravital microscopy, we could confirm in vivo that CD40 activation leads to the enhanced formation of ULVWF multimer–platelet strings. Although we could not identify vWF filaments under the experimental conditions given, we observed that the labeled platelets were forming pearl necklace-like structures (their gaps supposedly filled with endogenous platelets) which suggest their adhesion to and spatial organization by a filamentous structure. Their apparent length (defined only by platelets) was usually shorter than reported by others for directly observed ULVWF multimers in vivo (20), perhaps because labeled platelets did not always adhere to the very ends of the filaments. In agreement with the in vitro studies, stimulation of CD40 with sCD154 increased the number of such strings significantly. Leukocytes attached preferentially and initially to these sites. In the microcirculation, this occurred mainly in venules, the physiologic site of leukocyte extravasation. CD45, which we used for leukocyte labeling, is not specific for monocytes. Thus, our microcirculatory studies support a role for endothelial cell CD40 in ULVWF multimer–platelet string formation and subsequent leukocyte attachment in vivo.

In conclusion, the aforementioned findings suggest that CD154-induced formation of platelet-decorated ULVWF multimers on the luminal EC surface facilitates the trapping of circulating monocytes from the circulating blood. The ULVWF multimer-bound activated platelets bring the monocytes into close contact with the EC surface despite the rather fast flow in these conduit arterial blood vessels and promote their diapedesis. Our findings therefore shed some light on the role of platelets in atherosclerotic lesion formation in general and the functional impact of CD154–CD40–mediated release and deposition of ULVWF multimers on the luminal surface of ECs situated at atherosclerosis predilection sites of the arterial tree.

Since ADAMTS13 deficiency is known to have a distinct proinflammatory potential, we further investigated the extent to which it promotes ULVWF multimer formation and monocyte recruitment. Several case-control studies reported a possible association between ADAMTS13 plasma levels and atherosclerosis, as ADAMTS13 deficiency was found in patients with CAD (42), AMI (43), and ischemic stroke (44). However, they do not answer the question whether ADAMTS13 deficiency is a cause or rather a consequence of such atherosclerosis-related cardiovascular complications.

Our results showing a CAD-related but also age-dependent decrease in plasma ADAMTS13 activity are in line with the findings of other clinical trials (42, 45, 46). Among the patients with CAD, 63% had ADAMTS13 activity values between 40–80%

Table 2. Patients' baseline characteristics

	CAD patients, *n* = 70
Age, y, mean ± SD	70.3 ± 11.7
No. male (%)	45 (64.3)
No. with hypertension (%)	63 (90)
No. with hypercholesterolemia (%)	39 (55.7)
No. with diabetes mellitus (%)	24 (34.3)
No. smoking (%)	26 (37.1)
No. with BMI >25 kg/m^2 (%)	14 (20)
No. with ACS (%)	12 (17.1)
No. with STEMI (%)	2/12 (16.7)
No. with NSTEMI (%)	6/12 (50)
No. with UAP (%)	4/12 (33.3)
No. with elective procedure (%)	58 (82.9)
No. with PCI/stenting (%)	31 (44.3)
No. of vessels affected (%)	
1	17 (24.3)
2	10 (14.3)
3	43 (61.4)
Maximal degree of stenosis (%)	
25–49%	10 (14.3)
50–74%	15 (21.4)
≥75%	45 (64.3)

Hypertension and hypercholesterolemia were defined according to ESC guidelines (68). Patients suffered from the following comorbidities: peripheral artery disease (4.3%), moderate or severe valvular disease (11.4%), atrial fibrillation (10%), chronic renal failure (2.9%), and positive history for transient ischemic attack or stroke (4.3%). ACS, acute coronary syndrome; BMI, body mass index; NSTEMI, non–ST-elevation myocardial infarction; PCI, percutaneous coronary intervention; STEMI, ST-elevation myocardial infarction; UAP, unstable angina pectoris.

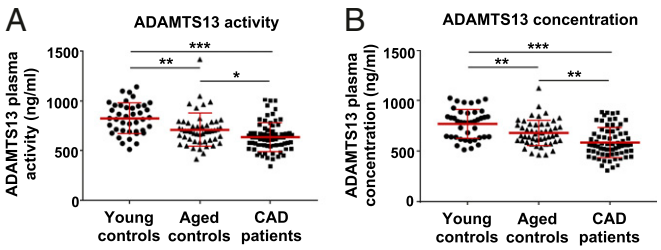

Fig. 5. ADAMTS13 plasma activity and antigen concentration in patients with CAD and healthy controls. ADAMTS13 activity and concentration levels were determined in platelet-poor plasma collected from CAD patients (n = 70) and were compared with ADAMTS13 levels in plasma of young (n = 41) and aged (n = 50) control groups with no history of CAD. Results are shown as scatter plots of individual measured values, mean ± SD being indicated by red bars. (*A*) Results of ADAMTS13 plasma activity as measured by a FRET assay. (*B*) ADAMTS13 antigen levels determined by ELISA. *P < 0.05, **P < 0.01, ***P < 0.001.

of normal activity, which also is consistent with previous reports (45). Importantly, plasma ADAMTS13 activity levels matched ADAMTS13 protein content in all three groups of patients and controls, suggesting that the CAD-related decrease in activity is not caused by expression of a dysfunctional protein by these individuals (e.g., as in patients with TTP) (47). Likewise, Bongers et al. (45) did not find an association between genetic variations of the ADAMTS13 gene and cardiovascular disease. What then causes the decrease in ADAMTS13 protein in patients with CAD? The cause might be endothelial dysfunction leading to enhanced release of ULVWF multimers, which causes depletion of ADAMTS13 plasma levels due to increased consumption (48). Owing to the long (3-d) half-life of ADAMTS13 in plasma (49), the plasma pool of ADAMTS13 after acute consumption due to endothelial dysfunction may be refilled rather slowly, so that the transitory ADAMTS13 deficiency becomes chronic. Furthermore, it is well known that proinflammatory cytokines such as TNF-α, IFN-γ, and IL-6 decrease ADAMTS13 expression and activity in ECs, hepatic stellate cells, and tumor microvessels (50). An important implication of these findings is that at sites of atherosclerotic lesions, which typically are characterized by increased production of these cytokines (51), ADAMTS13 production can be locally inhibited, thus promoting ULVWF multimer–platelet string formation.

Is the moderate decline in plasma ADAMTS13 activity in patients with CAD clinically relevant? Is ADAMTS13 deficiency directly involved in atherogenesis, or is it just a biomarker associated with the degree of inflammation? Although not yet determined for patients with cardiovascular disease, these are rather pressing questions from a medical point of view (22). Therefore we performed titration experiments with our cellular bioassay system to determine whether there is a threshold below which plasma ADAMTS13 activity would result in insufficient ULVWF multimer cleavage. In agreement with previous reports (52),we found that the ULVWF multimer-cleaving capacity of ADAMTS13 follows an exponential concentration–response curve with a threshold around 600 ng/mL, below which the protease is no longer capable of effectively cleaving the ULVWF multimer–platelet strings deposited on the surface of the cultured ECs. Superfusion of bradykinin-stimulated ECs with pooled native plasma from 24 patients with CAD enabled the formation of ULVWF multimer–platelet strings on the EC surface, an effect that was not observed with the pooled native plasma from 20 young healthy controls. This finding is highly relevant, as it clearly demonstrates that plasma of patients with CAD is unable to completely eliminate ULVWF multimers from the EC surface under flow. This effect is most probably attributable to ADAMTS13, since it is the only specific vWF-cleaving protease. However, other enzymes, such as leukocyte proteases, cathepsin G, elastase, granzyme B, and proteinase-3 (53–55), are also known to cleave vWF in vitro at fairly nonphysiological concentrations (22).

Finally, superfusion of CD154-stimulated ECs with reconstituted blood containing only 40% of the normal ADAMTS13 plasma concentration (350 ng/mL, as frequently found in the lowest quartile of the CAD cohort) enabled the formation of platelet-decorated ULVWF strings which were stable enough to subsequently trap circulating monocytes. In summary, these findings provide strong evidence for our hypothesis that platelet CD154-dependent monocyte recruitment and transmigration at atherosclerosis predilection sites in patients with CAD are reinforced by the release of ULVWF multimers from the ECs and exacerbated by moderate ADAMTS13 deficiency in the plasma.

It must be noted that the present study did not perform a subgroup analysis for comorbidities, risk factor constellations, and pharmacotherapy of CAD patients due to the small case numbers. However, the large prospective clinical trial of Miura et al. (42) showed that pharmacotherapy does not have an effect on ADAMTS13 and vWF levels. They also found no correlation with hypertension, smoking, or diabetes mellitus, suggesting that medication and other CAD risk factors do not affect ADAMTS13 levels. Another study limitation is that the aged control group was on average 7.2 y younger than the CAD group. This was due to recruitment limitations of volunteers above 70 y of age without cardiovascular disease, considering that the prevalence of cardiovascular disease in this age group is very high (69.1% in men and 67.9% in women aged 60–79 y) (56). Despite the statistically significant age difference, it is rather unlikely that the observed difference in ADAMTS13 between the two groups can be attributed entirely to age.

These findings may have important implications for understanding the relevance of ADAMTS13 in the context of atherosclerosis and its sequelae. Recent studies using ADAMTS13-knockout mouse models demonstrated a role for ADAMTS13 deficiency in atherogenesis (57) and in the development of acute

Table 3. Statistical data for ADAMTS13 plasma activity and plasma concentration in young controls, aged controls, and CAD patients

	n	ADAMTS13	Mean ± SD	Median	25th percentile	75th percentile	Minimum	Maximum
Young controls	41	Activity	823.7 ± 154.6*	823.5	696.3	949.8	511.4	1,140.0
		Concentration	770.6 ± 146.0	786.0	640.2	881.2	514.0	1,026.0
Aged controls	50	Activity	709.4 ± 166.8**	694.3	600.1	779.4	414.0	1,415.0
		Concentration	681.3 ± 127.7	668.1	601.9	763.9	462.2	1,124.0
CAD patients	70	Activity	636.3 ± 146.0	621.8	549.3	696.8	343.2	1,010.0
		Concentration	586.7 ± 146.6	561.0	480.5	681.1	308.5	887.9

All values are expressed in nanograms per milliliter.
*P < 0.001 vs. ADAMTS13 activity in CAD patients.
**P < 0.05 vs. ADAMTS13 activity in CAD patients.

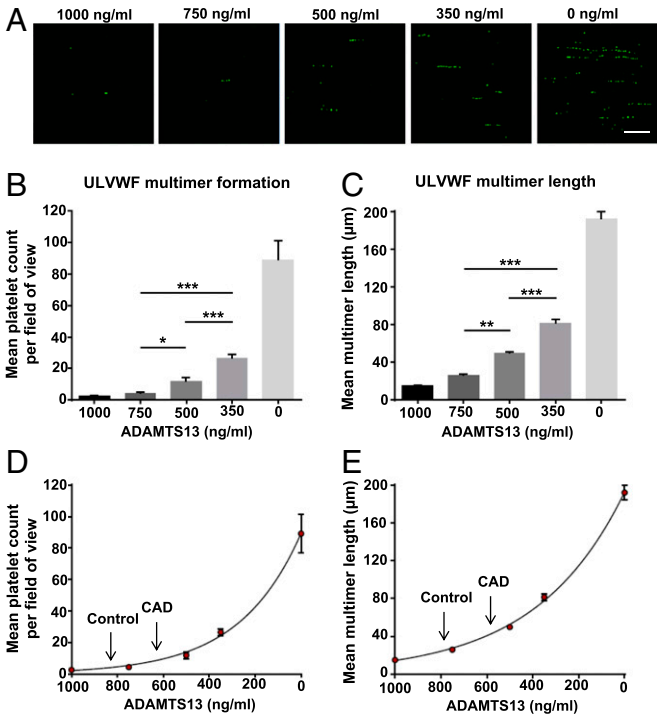

Fig. 6. Effect of different ADAMTS13 concentrations on ULVWF multimer formation and length. Titration experiments using different concentrations of ADAMTS13 were performed in the established perfusion system. HUVECs were superfused with an erythrocyte suspension containing serially diluted plasma collected from three healthy donors and green fluorescent-labeled platelets (2×10^6/mL) at 10 dyn/cm^2. ULVWF multimer formation was induced by stimulation with 100 nmol/L bradykinin. (*A*) Representative fields of view showing ULVWF string formation using the indicated ADAMTS13 concentrations. (Scale bar: 100 μm.) (*B* and *C*) Quantification of platelet adhesion (*B*) and ULVWF multimer length (*C*) at different ADAMTS13 concentrations. (*D* and *E*) Plotting of platelet count (*D*) and multimer length (*E*) values against ADAMTS13 concentrations revealed an exponential increase of these parameters and were approximated by exponential curves [R^2 = 0.8887 (*D*) and R^2 = 0.9838 (*E*)]. Arrows indicate the mean ADAMTS13 activity and concentration measured in CAD patient plasma and in young healthy controls, as shown in Table 3; $n = 5$; $^*P < 0.05$, $^{**}P < 0.01$, $^{***}P < 0.001$.

cardiovascular events such as AMI (58) or ischemic stroke (59). Herein we make this role tangible in patients with atherosclerosis and related cardiovascular diseases. Blocking P-selectin may represent a more feasible approach to inhibit platelet–monocyte interactions and to reduce atherosclerosis, as shown by several animal studies (60, 61) and two recent clinical trials which tested the newly developed anti–P-selectin antibody inclacumab (62, 63). In addition, platelet–vWF interactions can be blocked by specific antibodies targeting vWF GpIb (caplacizumab) and platelet GpIb receptor (anfibatide), which have recently been tested in phase I and phase II clinical trials with very promising results (64, 65). These not only would prevent thromboembolic complications upon plaque rupture but also may potentially inhibit platelet-mediated monocyte adhesion to ULVWF multimers deposited on the luminal EC surface. Thus, our bioassay approach may become a useful diagnostic tool to assess ADAMTS13 activity in the plasma of such patients under appropriate simulation of arterial blood flow conditions and seems to be more relevant than the conventional static FRET-based assay method (66).

Materials and Methods

Cell Culture. HUVECs were freshly isolated and cultured as described previously (67). Details regarding seeding, stimulation, and harvesting protocols are found in *SI Appendix*. For flow assays, HUVECs were seeded into ibidi flow chambers (μ-Slides I 0.4 Luer ibiTreat, ibidi) and were cultured under low oscillatory flow (±0.5 dyn/cm^2) for 5 d until an intact monolayer was formed. For application of orbital shear stress, HUVECs were grown in 12-well plates or specialized glass-bottomed dishes (35-mm dish, 20-mm glass diameter; MatTek) and were placed on top of an orbital shaker (100 rpm, corresponding to ∼3 dyn/cm^2) (7, 15).

Blood Collection and Plasma ADAMTS13 Quantification. Human whole blood from CAD patients and healthy volunteers was collected into citrate tubes (S-Monovette 10 mL 9 NC, 3.2% citrate; Sestet) by puncture of an antecubital vein with a 21-gauge needle according to the approval of the local ethics committee in Heidelberg (S-181/2013, S-689/2015). Seventy CAD patients admitted to Heidelberg University Hospital (Heidelberg) and the German Heart Centre (Munich) between August 2014 and April 2016 were eligible for participation in this study (Table 1). All subjects signed an informed consent. Samples were deidentified, and no identifiable personal information was included in this study. CAD patients satisfied inclusion criteria when showing angiographic evidence of ≥25% stenosis in a relevant coronary artery. Hypertension and hypercholesterolemia were defined according to current European Society of Cardiology (ESC) guidelines (68). Blood was drawn shortly before starting the elective cardiac catheterization. Genotyping of human blood for the T-786C NOS3 SNP was carried out as published previously (17). The young control group (Table 1) and the aged control group (Table1) consisted of healthy volunteers who had no history of cardiovascular diseases, were nonsmokers, and did not take any medication. Citrated platelet-poor plasma was obtained immediately by centrifugation (1,500 × *g*) and was stored at −80 °C until being assayed. ADAMTS13 plasma activity was measured in citrated platelet-poor plasma using a commercially available FRET-based activity assay (ACTIFLUOR ADAMTS13 Activity Assay; Sekisui Diagnostics). An

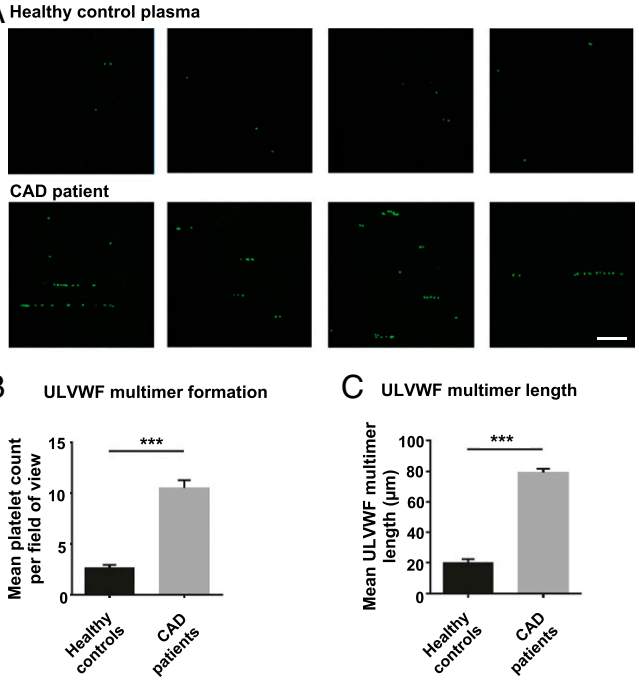

Fig. 7. Effect of CAD patient plasma on ULVWF multimer formation. Pooled platelet-poor plasma collected from 24 CAD patients and 20 young healthy controls was perfused in three independent experiments over HUVECs treated with 100 nmol/L bradykinin at 10 dyn/cm^2 using an erythrocyte suspension containing green fluorescent-labeled platelets (2×10^6/mL). Plasma samples were randomly selected from the groups recruited for ADAMTS13 plasma measurements. (*A*) Representative images of platelet adherence to ULVWF multimers on the endothelial cell surface upon perfusion with pooled plasma from healthy controls and from CAD patients. (Scale bar: 100 μm.) (*B* and *C*) Quantification of ULVWF multimer formation (*B*) and length (*C*) as observed during the first 10 min of perfusion; $n = 3$, $^{***}P < 0.001$.

ELISA (Human ADAMTS13 Quantikine ELISA Kit; R&D Systems) was employed to quantify ADAMTS13 plasma concentration.

Blood Cell Isolation. Human erythrocytes, platelets, and monocytes were isolated from freshly drawn citrated blood of healthy volunteers (18–65 y old) according to the approval of the local ethics committee. Erythrocytes were isolated by density gradient centrifugation, and platelet suspensions were prepared as described previously (69). A pure monocyte suspension was obtained by negative magnetic bead selection using the commercially available Pan Monocyte Isolation Kit (MACS; Miltenyi Biotec) as previously published (7). Flow cytometry for analysis of monocyte purity and monocyte and platelet labeling using fluorescent dyes are described in *SI Appendix*.

Flow Assay Setup. Confluent HUVECs cultured in flow chambers were exposed to defined unidirectional laminar shear stress (2.5 and 10 dyn/cm^2) using an ibidi pump system (ibidi). HUVECs were superfused for up to 60 min using a plasma-free reconstituted blood solution consisting of freshly isolated human erythrocytes (45% hematocrit), platelets (2×10^6/mL), and monocytes (0.8×10^6/mL). A more detailed description is found in *SI Appendix*. ULVWF multimer formation and platelet–monocyte interactions were analyzed in real time using live-cell imaging and RICM. A detailed description of these methods is found in *SI Appendix*.

Intravital Microscopy. The animal experiments were performed in accordance with the German animal protection law and had been approved by the district government of upper Bavaria. The investigation conforms to the European Commission Directive 2010/63/EU. Cremaster muscles of ADAMSTS13-knockout mice (stock: 007235; Jackson Laboratories) and C57BL/6J as wild-type control mice were prepared for intravital microscopy as described before (70). The endothelium of arterioles and venules was labeled by topical application of Alexa Fluor 647-labeled CD31 antibody (BD Biosciences) for 1 h. Platelets from C57/BL6 donor animals were washed and labeled ex vivo with carboxyfluorescein diacetate (CFDA) as described earlier (71). Two hundred-microliter platelet suspensions corresponding to 8×10^6 platelets were injected into the circulation. Circulating leukocytes were labeled by i.v. injection of a PE-CD45 antibody (eBioscience). The cremaster blood vessels were stimulated by adding 5 μg recombinant sCD40L dissolved in 50 μL of saline solution to the supernatant for 20 min. Images were obtained for an observation period of up to 120 min by two-photon excitation microscopy (TriM Scope; LaVision BioTech). Images were stored and analyzed off-line using IMARIS software (Bitplane).

Real-Time PCR, Western Blot, and Immunocytochemistry Analysis. Real-time qPCR analysis of relative mRNA expression was conducted as described previously (72). Western blot analysis was performed using standard protocols. PCR primer pairs and Western blot antibodies used for protein quantification are listed in *SI Appendix*. Immunofluorescence staining of fixed HUVECs was conducted as described previously (73) using antibodies for vWF (F3520; Sigma-Aldrich) and VE-cadherin (sc-6458; Santa Cruz Biotechnology). Perfused μ-slides were fixed under flow and subsequently stained according to the standard protocol. Fluorescence intensity and the number of nuclei were quantitated using ImageJ software (1.45r).

Statistical Analysis. Statistical analysis was performed using GraphPad Prism 6.0 software. Unpaired Student's *t* tests were used for two-group comparisons, and one-sample *t* tests were used for values expressed as relative to a control sample. For data encompassing three or more groups, one-way ANOVA with Tukey's multiple comparisons test was employed. *P* values <0.05 were considered statistically significant.

ACKNOWLEDGMENTS. We thank Dr. Gerd König for careful and excellent revision of the manuscript and Franziska Mohr and Nadine Heselmaier for expert technical assistance. This work was supported by Deutsche Forschungsgemeinschaft Collaborative Research Centre (CRC) Transregio 23 Subproject C6, the European Commission Marie Curie Innovative Training Network SmArteR Project, and German CRC Project 81X2500110.

1. Galkina E, Ley K (2009) Immune and inflammatory mechanisms of atherosclerosis (*). *Annu Rev Immunol* 27:165–197.
2. Moore KJ, Sheedy FJ, Fisher EA (2013) Macrophages in atherosclerosis: A dynamic balance. *Nat Rev Immunol* 13:709–721.
3. Tedgui A, Mallat Z (2006) Cytokines in atherosclerosis: Pathogenic and regulatory pathways. *Physiol Rev* 86:515–581.
4. Mach F, Schönbeck U, Sukhova GK, Atkinson E, Libby P (1998) Reduction of atherosclerosis in mice by inhibition of CD40 signalling. *Nature* 394:200–203.
5. Lievens D, Eijgelaar WJ, Biessen EA, Daemen MJ, Lutgens E (2009) The multi-functionality of CD40L and its receptor CD40 in atherosclerosis. *Thromb Haemost* 102:206–214.
6. Sadler JE (1998) Biochemistry and genetics of von Willebrand factor. *Annu Rev Biochem* 67:395–424.
7. Möller K, et al. (2015) Mechanism and functional impact of CD40 ligand-induced von Willebrand factor release from endothelial cells. *Thromb Haemost* 113:1095–1108.
8. Springer TA (2014) von Willebrand factor, Jedi knight of the bloodstream. *Blood* 124: 1412–1425.
9. Dong JF (2005) Cleavage of ultra-large von Willebrand factor by ADAMTS-13 under flow conditions. *J Thromb Haemost* 3:1710–1716.
10. Zheng X, et al. (2001) Structure of von Willebrand factor-cleaving protease (ADAMTS13), a metalloprotease involved in thrombotic thrombocytopenic purpura. *J Biol Chem* 276:41059–41063.
11. Tsai HM (2010) Pathophysiology of thrombotic thrombocytopenic purpura. *Int J Hematol* 91:1–19.
12. Henn V, et al. (1998) CD40 ligand on activated platelets triggers an inflammatory reaction of endothelial cells. *Nature* 391:591–594.
13. Furman MI, et al. (1998) Increased platelet reactivity and circulating monocyte-platelet aggregates in patients with stable coronary artery disease. *J Am Coll Cardiol* 31:352–358.
14. Ley K, Laudanna C, Cybulsky MI, Nourshargh S (2007) Getting to the site of inflammation: The leukocyte adhesion cascade updated. *Nat Rev Immunol* 7:678–689.
15. Potter CM, et al. (2011) Role of shear stress in endothelial cell morphology and expression of cyclooxygenase isoforms. *Arterioscler Thromb Vasc Biol* 31:384–391.
16. Benjamin EJ, et al.; American Heart Association Statistics Committee and Stroke Statistics Subcommittee (2017) Heart disease and stroke statistics-2017 update: A report from the American Heart Association. *Circulation* 135:e146–e603.
17. Cattaruzza M, et al. (2004) Shear stress insensitivity of endothelial nitric oxide synthase expression as a genetic risk factor for coronary heart disease. *Circ Res* 95: 841–847.
18. Lutgens E, et al. (2010) Deficient CD40-TRAF6 signaling in leukocytes prevents atherosclerosis by skewing the immune response toward an antiinflammatory profile. *J Exp Med* 207:391–404.
19. Chauhan AK, Goerge T, Schneider SW, Wagner DD (2007) Formation of platelet strings and microthrombi in the presence of ADAMTS-13 inhibitor does not require P-selectin or β3 integrin. *J Thromb Haemost* 5:583–589.
20. Dong JF, et al. (2002) ADAMTS-13 rapidly cleaves newly secreted ultralarge von Willebrand factor multimers on the endothelial surface under flowing conditions. *Blood* 100:4033–4039.
21. Huang J, Roth R, Heuser JE, Sadler JE (2009) Integrin alpha(v)beta(3) on human endothelial cells binds von Willebrand factor strings under fluid shear stress. *Blood* 113: 1589–1597.
22. De Ceunynck K, De Meyer SF, Vanhoorelbeke K (2013) Unwinding the von Willebrand factor strings puzzle. *Blood* 121:270–277.
23. Huck V, Schneider MF, Gorzelanny C, Schneider SW (2014) The various states of von Willebrand factor and their function in physiology and pathophysiology. *Thromb Haemost* 111:598–609.
24. Tayebjee MH, et al. (2005) Plasma matrix metalloproteinase-9, tissue inhibitor of metalloproteinase-2, and CD40 ligand levels in patients with stable coronary artery disease. *Am J Cardiol* 96:339–345.
25. Wang Y, et al. (2007) Transcoronary concentration gradient of sCD40L and hsCRP in patients with coronary heart disease. *Clin Cardiol* 30:86–91.
26. Tousoulis D, Antoniades C, Stefanadis C (2007) Assessing inflammatory status in cardiovascular disease. *Heart* 93:1001–1007.
27. Antoniades C, Bakogiannis C, Tousoulis D, Antonopoulos AS, Stefanadis C (2009) The CD40/CD40 ligand system: Linking inflammation with atherothrombosis. *J Am Coll Cardiol* 54:669–677.
28. van Gils JM, Zwaginga JJ, Hordijk PL (2009) Molecular and functional interactions among monocytes, platelets, and endothelial cells and their relevance for cardiovascular diseases. *J Leukoc Biol* 85:195–204.
29. Pendu R, et al. (2006) P-selectin glycoprotein ligand 1 and beta2-integrins cooperate in the adhesion of leukocytes to von Willebrand factor. *Blood* 108:3746–3752.
30. Bernardo A, et al. (2005) Platelets adhered to endothelial cell-bound ultra-large von Willebrand factor strings support leukocyte tethering and rolling under high shear stress. *J Thromb Haemost* 3:562–570.
31. De Maeyer B, et al. (2010) The distal carboxyterminal domains of murine ADAMTS13 influence proteolysis of platelet-decorated VWF strings in vivo. *J Thromb Haemost* 8:2305–2312.
32. Bauer HM (1975) In-vitro platelet-neutrophil adherence. *Am J Clin Pathol* 63:824–827.
33. Ott I, Neumann FJ, Gawaz M, Schmitt M, Schömig A (1996) Increased neutrophil-platelet adhesion in patients with unstable angina. *Circulation* 94:1239–1246.
34. Setianto BY, Hartopo AB, Gharini PP, Anggrahini DW, Irawan B (2010) Circulating soluble CD40 ligand mediates the interaction between neutrophils and platelets in acute coronary syndrome. *Heart Vessels* 25:282–287.
35. Zawada AM, et al. (2012) Monocyte heterogeneity in human cardiovascular disease. *Immunobiology* 217:1273–1284.
36. Springer TA (1994) Traffic signals for lymphocyte recirculation and leukocyte emigration: The multistep paradigm. *Cell* 76:301–314.
37. Yeo EL, Sheppard JA, Feuerstein IA (1994) Role of P-selectin and leukocyte activation in polymorphonuclear cell adhesion to surface adherent activated platelets under physiologic shear conditions (an injury vessel wall model). *Blood* 83:2498–2507.

38. Kuligowski MP, Kitching AR, Hickey MJ (2006) Leukocyte recruitment to the inflamed glomerulus: A critical role for platelet-derived P-selectin in the absence of rolling. *J Immunol* 176:6991–6999.
39. da Costa Martins PA, van Gils JM, Mol A, Hordijk PL, Zwaginga JJ (2006) Platelet binding to monocytes increases the adhesive properties of monocytes by up-regulating the expression and functionality of beta1 and beta2 integrins. *J Leukoc Biol* 79:499–507.
40. Huo Y, et al. (2003) Circulating activated platelets exacerbate atherosclerosis in mice deficient in apolipoprotein E. *Nat Med* 9:61–67.
41. van Gils JM, da Costa Martins PA, Mol A, Hordijk PL, Zwaginga JJ (2008) Transendothelial migration drives dissociation of plateletmonocyte complexes. *Thromb Haemost* 100:271–279.
42. Miura M, et al. (2010) Prognostic value of plasma von Willebrand factor-cleaving protease (ADAMTS13) antigen levels in patients with coronary artery disease. *Thromb Haemost* 103:623–629.
43. Crawley JT, Lane DA, Woodward M, Rumley A, Lowe GD (2008) Evidence that high von Willebrand factor and low ADAMTS-13 levels independently increase the risk of a non-fatal heart attack. *J Thromb Haemost* 6:583–588.
44. Lambers M, et al. (2013) Role of reduced ADAMTS13 in arterial ischemic stroke: A pediatric cohort study. *Ann Neurol* 73:58–64.
45. Bongers TN, et al. (2009) Lower levels of ADAMTS13 are associated with cardiovascular disease in young patients. *Atherosclerosis* 207:250–254.
46. Kaikita K, Soejima K, Matsukawa M, Nakagaki T, Ogawa H (2006) Reduced von Willebrand factor-cleaving protease (ADAMTS13) activity in acute myocardial infarction. *J Thromb Haemost* 4:2490–2493.
47. Kokame K, et al. (2002) Mutations and common polymorphisms in ADAMTS13 gene responsible for von Willebrand factor-cleaving protease activity. *Proc Natl Acad Sci USA* 99:11902–11907.
48. Claus RA, Bockmeyer CL, Sossdorf M, Lösche W (2010) The balance between von-Willebrand factor and its cleaving protease ADAMTS13: Biomarker in systemic inflammation and development of organ failure? *Curr Mol Med* 10:236–248.
49. Furlan M, Robles R, Morselli B, Sandoz P, Lämmle B (1999) Recovery and half-life of von Willebrand factor-cleaving protease after plasma therapy in patients with thrombotic thrombocytopenic purpura. *Thromb Haemost* 81:8–13.
50. Bauer AT, et al. (2015) von Willebrand factor fibers promote cancer-associated platelet aggregation in malignant melanoma of mice and humans. *Blood* 125: 3153–3163.
51. Frostegård J, et al. (1999) Cytokine expression in advanced human atherosclerotic plaques: Dominance of pro-inflammatory (Th1) and macrophage-stimulating cytokines. *Atherosclerosis* 145:33–43.
52. Zhang X, Halvorsen K, Zhang CZ, Wong WP, Springer TA (2009) Mechanoenzymatic cleavage of the ultralarge vascular protein von Willebrand factor. *Science* 324: 1330–1334.
53. Tsai HM, Nagel RL, Hatcher VB, Sussman II (1989) Endothelial cell-derived high molecular weight von Willebrand factor is converted into the plasma multimer pattern by granulocyte proteases. *Biochem Biophys Res Commun* 158:980–985.
54. Buzza MS, et al. (2008) Antihemostatic activity of human granzyme B mediated by cleavage of von Willebrand factor. *J Biol Chem* 283:22498–22504.
55. Jeleńska M, et al. (1991) Fibrinogen does not protect von Willebrand factor against proteolysis by human cathepsin G. *Thromb Res* 61:433–440.
56. Mozaffarian D, et al.; American Heart Association Statistics Committee and Stroke Statistics Subcommittee (2015) Heart disease and stroke statistics–2015 update: A report from the American Heart Association. *Circulation* 131:e29–e322.
57. Gandhi C, Ahmad A, Wilson KM, Chauhan AK (2014) ADAMTS13 modulates atherosclerotic plaque progression in mice via a VWF-dependent mechanism. *J Thromb Haemost* 12:255–260.
58. De Meyer SF, et al. (2012) Protective anti-inflammatory effect of ADAMTS13 on myocardial ischemia/reperfusion injury in mice. *Blood* 120:5217–5223.
59. Fujioka M, et al. (2010) ADAMTS13 gene deletion aggravates ischemic brain damage: A possible neuroprotective role of ADAMTS13 by ameliorating postischemic hypoperfusion. *Blood* 115:1650–1653.
60. Johnson RC, et al. (1997) Absence of P-selectin delays fatty streak formation in mice. *J Clin Invest* 99:1037–1043.
61. Dong ZM, Brown AA, Wagner DD (2000) Prominent role of P-selectin in the development of advanced atherosclerosis in ApoE-deficient mice. *Circulation* 101: 2290–2295.
62. Kling D, et al. (2013) Pharmacological control of platelet-leukocyte interactions by the human anti-P-selectin antibody inclacumab–Preclinical and clinical studies. *Thromb Res* 131:401–410.
63. Schmitt C, et al. (2015) First-in-man study with inclacumab, a human monoclonal antibody against P-selectin. *J Cardiovasc Pharmacol* 65:611–619.
64. Peyvandi F, et al.; TITAN Investigators (2016) Caplacizumab for acquired thrombotic thrombocytopenic purpura. *N Engl J Med* 374:511–522.
65. Hou Y, et al. (2013) The first in vitro and in vivo assessment of anfibatide, a novel glycoprotein Ib antagonist, in mice and in a phase I human clinical trial. *Blood* 122: 577.
66. Zhang P, Pan W, Rux AH, Sachais BS, Zheng XL (2007) The cooperative activity between the carboxyl-terminal TSP1 repeats and the CUB domains of ADAMTS13 is crucial for recognition of von Willebrand factor under flow. *Blood* 110:1887–1894.
67. Lienenlüke B, Germann T, Kroczek RA, Hecker M (2000) CD154 stimulation of interleukin-12 synthesis in human endothelial cells. *Eur J Immunol* 30:2864–2870.
68. Montalescot G, et al.; Task Force Members; ESC Committee for Practice Guidelines; Document Reviewers (2013) 2013 ESC guidelines on the management of stable coronary artery disease: The Task Force on the management of stable coronary artery disease of the European Society of Cardiology. *Eur Heart J* 34:2949–3003.
69. Cazenave JP, et al. (2004) Preparation of washed platelet suspensions from human and rodent blood. *Methods Mol Biol* 272:13–28.
70. Mannell HK, et al. (2012) ARNO regulates VEGF-dependent tissue responses by stabilizing endothelial VEGFR-2 surface expression. *Cardiovasc Res* 93:111–119.
71. Koch E, et al. (2013) The endothelial tyrosine phosphatase SHP-1 plays an important role for vascular haemostasis in TNFα -induced inflammation in vivo. *Mediators Inflamm* 2013:279781.
72. Wagner AH, Güldenzoph B, Lienenlüke B, Hecker M (2004) CD154/CD40-mediated expression of CD154 in endothelial cells: Consequences for endothelial cell-monocyte interaction. *Arterioscler Thromb Vasc Biol* 24:715–720.
73. Wagner AH, et al. (2011) Tyrosine nitration limits stretch-induced CD40 expression and disconnects CD40 signaling in human endothelial cells. *Blood* 118:3734–3742.